Engineering Analysis with Boundary Elements 34 (2010) 775–784

Contents lists available at ScienceDirect

Engineering Analysis with Boundary Elements

journal homepage: www.elsevier.com/locate/enganabound

Boundary element analysis of the thermal behaviour in thin-coated cutting tools

Yaoming Zhang [a,*], Yan Gu [a], Jeng-Tzong Chen [b]

[a] Institute of Applied Mathematics, Shandong University of Technology, Zibo 255049, Shandong Province, China
[b] Department of Harbor and River Engineering, National Taiwan Ocean University, Keelung 20224, Taiwan

ARTICLE INFO

Article history:
Received 28 February 2010
Accepted 30 March 2010
Available online 15 May 2010

Keywords:
Tool coating
Temperature distributions
Boundary element method
Transformation
Nearly singular integrals
Thin body
High-order geometry element

ABSTRACT

Temperature measurement and prediction have been a major focus of machining for several decades, but now these problems become more complex due to the wider use of advanced cutting tool coatings. In all literature items cited the boundary element method (BEM) were used to find the distribution of temperature inside the uncoated tool body or along the tool–chip interface in the machining processes. The BEM-based approach proposed in this paper overcomes this limit and the temperature distribution in thin coated layers is well studied. In this study, a general strategy based on a nonlinear transformation technique is introduced and applied to evaluate the nearly singular integrals occurring in two dimensional (2D) thin-coated structures. For the test problems studied, very promising results are obtained when the thickness to length ratio is in the orders of 1.0E−6 to 1.0E−10, which is sufficient for modeling most thin-coated structures in the micro- or nano-sclaes.

1. Introduction

Following improvements in coating deposition techniques and the development of more advanced coating materials, more and more thin-coating films are being designed and utilized in industrial applications to improve machining performance due to better temperature and wear resistant properties than their substrate counterparts. During machining processes, heat is a source that strongly influences the tool performance. The cutting temperature field determines key process issues such as many parameters including accuracy of the machined surface, tool wear, tool life, mechanics of chip formation, surface quality, and cutting forces as well as process quality [1]. The coatings of cutting tools have significant influence on heat conduction in the tools during machining. Thus, having a clear understanding about the temperature distribution in coated cutting tools is very useful and important. However, the widespread experimental research in coatings underlies a general lack of modeling efforts, which represents a great challenge to researchers in computational mechanics.

It is well-known that the thermal model of heat conduction in coated tools have been performed by utilizing experimental, analytical and numerical methods. The usual numerical methods such as the finite element method (FEM), the finite difference method (FDM) and the boundary element method (BEM) can be applied to solve heat transfer problems in cutting tools. The FEM is a successful tool for the analysis of many industrial problems. However, the number of elements in FEM increases dramatically for thin structures due to aspect ratio limitations, and the procedure therefore requires much preprocessing and CPU time as the thickness decreases. BEM is a powerful and efficient computational method if boundary integrals can be evaluated accurately. The main advantage of the BEM resulting from the reduction of the dimension of the boundary value problem is well-known. However, it is popular as well that the standard BEM formulations include singular and nearly singular integrals, and thus the integrations should be performed very carefully. In the area of calculation of temperature distributions for cutting tools, several researchers have recently utilized the boundary element method. In the pioneering work in this area, Chandra and Chan [2] solved the steady-state heat conduction problem by using a two-dimensional boundary element method. Stephenson et al. [3] later expanded Chandra and Chan's work to perform numerical simulations of transient heat conduction problems in the machining using a three-dimensional boundary element method. In a more recent work, Du et al. [4] proposed two techniques to determine the temperature fields in materials containing thin coatings. The first method utilizes a multi-domain approach, but this method is inefficient when the coating is very thin due to the lack of efficient techniques to calculate the nearly singular integrals. The second technique, which is based on the finite difference approximation, is geared towards applications where the coating thickness is very small. However, the temperature distribution in thin-coated layers is not given in their work.

* Corresponding author.
E-mail address: zymfc@163.com (Y. Zhang).

0955-7997/$ - see front matter © 2010 Elsevier Ltd. All rights reserved.
doi:10.1016/j.enganabound.2010.03.014

Despite the significant contributions of each of the above works, it is important to note that they were all focused on observing the distribution of temperature inside the uncoated tool body or along the tool–chip interface. To the author's best knowledge, we do not find any work in the literature for determining the temperature distribution in the thin-coated layers, which is obviously more important in the manufacturing community. The objective of this paper is to develop a general BEM-based simulation for predicting the temperature distribution in thin-coated layers as well as in their substrate counterparts.

In the authors' opinion, the following three major concerns must be well addressed in applying the BEM to thin-coated structural problems: (1) Calculating the singular integrals accurately. It is well-known that the domain variables can be computed by integral equations after all the boundary quantities have been obtained, and the accuracy of boundary quantities directly affects the validity of the interior quantities. Therefore, we have to deal with the singular boundary integrals when calculating the boundary quantities and a good choice is using the regularized boundary integral equations (BIEs) [5–15]. (2) Using high-order geometry element. The advantage of using high-order geometry elements in thin structural problems is the concerning power to improve the calculation accuracy. More importantly, computational models of thin structural problems demand a higher level of the geometry approximation, and the usage of high-order geometry in computational models can meet this requirement. For example, if the boundary geometry is depicted by using the straight line, the linear element of the outer surface will attach (*AB*) or even pass through (*CD*) the inner boundary if the thickness of the considered structure is very small (Fig. 1). Consequently, the actual geometry of considered domain cannot be described lively, and thus lower-order geometry approximation will fail to yield reliable results for such problems. In order to avoid this phenomenon, very fine meshes mush be used in this situation, but this yields too much preprocessing and CPU time. In addition, a great number of meshes will produce a lot of artificial corners that will lead to the uncontinuity of the tangent derivative of the boundary unknowns. This is fatal to many engineering problems. (3) Calculating the nearly singular integrals accurately. It is well-known that the conventional BIE using the standard Gaussian quadrature fails to yield reliable results for thin structural problems. The major reason for this failure is that the conventional BIE not only includes singular integrals but also presents various orders of near singularities, owing to the mesh on one side of the thin body being too close to the mesh on the opposite side. Moreover, since all the interior points of thin bodies are very close to the boundary, the calculation of nearly singular integrals is also inevitable when physical quantities at an interior point need to be calculated.

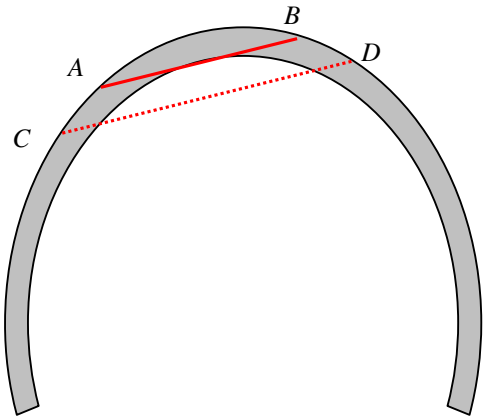

Fig. 1. A thin-walled structure with illogical geometry element.

The nearly singular integrals are not singular in the sense of mathematics. However, from the point of view of numerical integrations, these integrals cannot be calculated accurately by using the conventional numerical quadrature since the integrand oscillates seriously within the integration interval. Although that difficulty can be overcome by using very fine meshes, the process requires too much preprocessing and CPU time. In the past decades, tremendous effort was devoted to derive convenient integral forms or sophisticated computational techniques for calculating the nearly singular integrals. These proposed methods can be divided on the whole into two categories: "indirect algorithms" and "direct algorithms". The indirect algorithms, which benefit from the regularization ideas and techniques for the singular integrals, are mainly adopted to calculate indirectly or avoid calculating the nearly singular integrals by establishing new regularized BIE [15–19]. The direct algorithms are employed to calculate the nearly singular integrals directly. They usually include interval subdivision method [20,21], special Gaussian quadrature method [22], exact integration method [23–26], and various nonlinear transformation methods [27–35]. In a recent study, the above methods have been reviewed in detail by Zhang and Sun [34]. It is noteworthy that Sladek et al. early discussed the regularization of the nearly singular integrals by using nonlinear transformations. An effective transformation based on the function $x=\sinh y$ is proposed in Refs. [7, pp. 387–392] and [29]. The transformation proposed in this paper is inspired by the previous works of the above researches.

Although great progresses have been achieved for each of the above methods, it should be pointed out that the geometry of the boundary element is often depicted by using linear shape functions when nearly singular integrals need to be calculated [35,36]. In fact, to the authors' best knowledge, no work is found in the literature that can be used to calculate the nearly singular integrals under high-order geometry effectively. However, as mentioned above, computational models of thin structural problems demand a higher level of the geometry approximation, and the usage of high-order geometry in computational models can meet this requirement. When the geometry of the boundary element is approximated by using high-order elements—usually of second order, the Jacobian $J(\xi)$ is not a constant but a non-rational function, which can be expressed as $\sqrt{a+b\xi+c\xi^2}$, where a, b, and c are constants, ξ is the dimensionless coordinate. The distance r between the field points and the source point is a non-rational function of the type $\sqrt{p_4(\xi)}$, where $p_4(\xi)$ is the fourth order polynomial. Thus, the forms of the integrands in boundary integrals become more complex, and it is, unfortunately, more difficult to implement when nearly singular integrals need to be calculated.

In this work, a general BEM-based method is introduced for evaluating the temperature field in a material containing a thin-layered coating. The main work of this paper can be summarized as follows: (1) introduce the regularized indirect BIEs to estimate the singular integrals on curved boundaries. It is important to note that the regularized BIEs only apply within each layer of material separately because of differences in thermal conductivity. Thus, a two-dimensional multi-domain boundary approach, which is applicable for a wide range of coating thicknesses, is utilized in this paper; (2) a general nonlinear transformation is adopted to remove or damp out the near singularities of kernels' integration by smoothing out the rapid variations of the integrand of nearly singular integrals. The present general nonlinear transformation is available for high-order geometry elements, which can meet the rigorous requirement of the model of complex thin structural problems in industrial applications.

The temperature distributions both in thin coated layers and its substrate counterparts are well studied. For the test problems studied, very promising results are obtained when the thickness to length ratio of the coatings in the orders of 1E−01 to 1E−10, which is sufficient for modeling most thin coated cutting tools in the micro- or nano-scales. The algorithm derived in this paper substantially simplifies the programming and provided a general computational method for solving thin coating problems.

2. Non-singular boundary integral equations (BIEs)

It is well-known that the domain variables would be computed by using integral equations only after all the boundary quantities have been obtained, and the accuracy of boundary quantities directly affects the validity of the interior quantities. However, when calculating the boundary quantities, we have to deal with the singular boundary integrals, and a good choice is to use the regularized BIEs. In this paper, we always assume that Ω is a bounded domain in R^2, Ω^c is its open complement; $\Gamma=\partial\Omega$ denotes their common boundary; $\boldsymbol{t}(\boldsymbol{x})$ and $\boldsymbol{n}(\boldsymbol{x})$ are the unit tangent and outward normal vectors of Γ to domain Ω at point $\boldsymbol{x}$, respectively. The temperature field in the cutting tool is governed by the Laplace's equation $\nabla^2 u=0$. For two dimensional potential problems, the equivalent non-singular BIEs with indirect variables are given in Ref. [14]. For the domain Ω, the equations are given as

$$\int_\Gamma \phi(\boldsymbol{x})d\boldsymbol{\Gamma}_x+\int_\Omega f(\boldsymbol{x})d\boldsymbol{\Omega}=0 \tag{1}$$

$$u(\boldsymbol{y})=\int_\Gamma \phi(\boldsymbol{x})u^*(\boldsymbol{x},\boldsymbol{y})d\Gamma+\int_\Omega f(\boldsymbol{x})u^*(\boldsymbol{x},\boldsymbol{y})d\Omega+C,\boldsymbol{y}\in\Gamma \tag{2}$$

$$\begin{aligned}\nabla u(\boldsymbol{y})=&\, n(\boldsymbol{y})\phi(\boldsymbol{y})+\textstyle\int_\Gamma[\phi(\boldsymbol{x})-\phi(\boldsymbol{y})]\nabla u^*(\boldsymbol{x},\boldsymbol{y})d\boldsymbol{\Gamma}\\ &-\phi(\boldsymbol{y})\left\{\int_\Gamma[\boldsymbol{t}(\boldsymbol{x})-\boldsymbol{t}(\boldsymbol{y})]\frac{\partial u^*(\boldsymbol{x},\boldsymbol{y})}{\partial \boldsymbol{t}_x}d\boldsymbol{\Gamma}\right.\\ &\left.+\int_\Gamma[\boldsymbol{n}(\boldsymbol{x})-\boldsymbol{n}(\boldsymbol{y})]\frac{\partial u^*(\boldsymbol{x},\boldsymbol{y})}{\partial \boldsymbol{n}_x}d\boldsymbol{\Gamma}\right\}+\int_\Omega f(\boldsymbol{x})\nabla u^*(\boldsymbol{x},\boldsymbol{y})d\boldsymbol{\Omega},\quad \boldsymbol{y}\in\boldsymbol{\Gamma}\end{aligned} \tag{3}$$

where $u^*(\boldsymbol{x},\boldsymbol{y})=-(1/2\pi)\ln r$ is the fundamental solution in two dimension problems.

For the domain Ω^c, the equations are given as

$$\int_\Gamma \phi(\boldsymbol{x})d\boldsymbol{\Gamma}_{\boldsymbol{x}}+\int_{\Omega_c} f(\boldsymbol{x})d\boldsymbol{\Omega}^c=0 \tag{4}$$

$$u(\boldsymbol{y})=\int_\Gamma \phi(\boldsymbol{x})u^*(\boldsymbol{x},\boldsymbol{y})\,d\boldsymbol{\Gamma}_{\boldsymbol{x}}+\int_{\Omega^c} f(\boldsymbol{x})u^*(\boldsymbol{x},\boldsymbol{y})\,d\boldsymbol{\Omega}^c+C,\boldsymbol{y}\in\boldsymbol{\Gamma} \tag{5}$$

$$\begin{aligned}\nabla_{\boldsymbol{y}}u(\boldsymbol{y})=&\textstyle\int_\Gamma[\phi(\boldsymbol{x})-\phi(\boldsymbol{y})]\nabla_{\boldsymbol{y}}u^*(\boldsymbol{x},\boldsymbol{y})d\boldsymbol{\Gamma}_{\boldsymbol{x}}\\ &-\phi(\boldsymbol{y})\left\{\int_\Gamma[\boldsymbol{t}^c(\boldsymbol{x})-\boldsymbol{t}^c(\boldsymbol{y})]\nabla u^*(\boldsymbol{x},\boldsymbol{y})\cdot\boldsymbol{t}^c(\boldsymbol{x})d\boldsymbol{\Gamma}_{\boldsymbol{x}}\right.\\ &\left.+\int_\Gamma[\boldsymbol{n}^c(\boldsymbol{x})-\boldsymbol{n}^c(\boldsymbol{y})]\nabla u^*(\boldsymbol{x},\boldsymbol{y})\cdot\boldsymbol{n}^c(\boldsymbol{x})d\boldsymbol{\Gamma}_{\boldsymbol{x}}\right\}\\ &+\int_{\Omega^c} f(\boldsymbol{x})\nabla_{\boldsymbol{y}}u^*(\boldsymbol{x},\boldsymbol{y})d\boldsymbol{\Omega}^c,\boldsymbol{y}\in\boldsymbol{\Gamma}.\end{aligned} \tag{6}$$

where $\boldsymbol{t}^c(\boldsymbol{x})$ and $\boldsymbol{n}^c(\boldsymbol{x})$ are the unit tangent and outward normal vectors of Γ to domain Ω^c at point $\boldsymbol{x}$, respectively.

For the internal point $\boldsymbol{y}$, the integral equations can be expressed as

$$u(\boldsymbol{y})=\int_\Gamma \phi(\boldsymbol{x})u^*(\boldsymbol{x},\boldsymbol{y})d\Gamma_x+\int_{\hat\Omega} f(\boldsymbol{x})u^*(\boldsymbol{x},\boldsymbol{y})d\hat\Omega+C,\boldsymbol{y}\in\hat\Omega \tag{7}$$

$$\nabla_{\boldsymbol{y}}u(\boldsymbol{y})=\int_\Gamma \phi(\boldsymbol{x})\nabla_{\boldsymbol{y}}u^*(\boldsymbol{x},\boldsymbol{y})d\Gamma_{\boldsymbol{x}}+\int_{\hat\Omega} f(\boldsymbol{x})\nabla_{\boldsymbol{y}}u^*(\boldsymbol{x},\boldsymbol{y})d\hat\Omega,\boldsymbol{y}\in\hat\Omega. \tag{8}$$

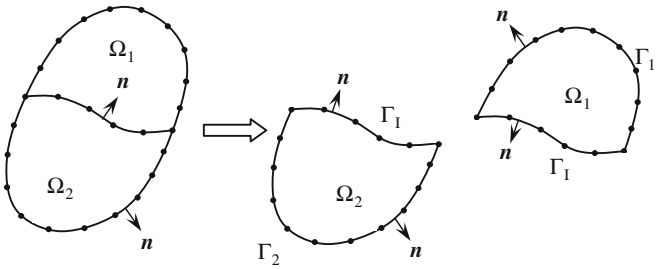

Fig. 2. Boundary discretization for two subdomains.

In Eqs. (1)–(8), $\phi(\boldsymbol{x})$ is the density function to be determined; $f(\boldsymbol{x})$ is the body function, and in Eqs. (7) and (8) $\hat\Omega=\Omega$ or Ω^c. It is important to note that in coated cutting tools, Eqs. (1)–(8) only apply within each layer of material separately because of differences in thermal conductivity.

In the machining industry, the coatings consist of one layer or more layers. Thin layers of coating protect the tool against adhesion, diffusion and intensive abrasive wear. They also provide a barrier for the intensive heat flow from the contact area into the substrate material. One way to model the tool containing coatings is to use the multi-domain BEM. In order to make this procedure clearer, only one layer of coating is treated in this paper. Although the formulation can be extended to multiple layers, the solution for multi-coating systems will merely increase the number of the equation, and we encounter no difficulty. A generic two domains problem is illustrated in Fig. 2 where the entire domain is composed of two homogenous and isotropic subdomains Ω_1 and Ω_2. The exterior boundary of subdomain Ω_1 is Γ_1 and that of subdomain Ω_2 is Γ_2. The contact interface between the two subdomains is Γ_I. The coefficients of heat conductivity of two subdomains are denoted by k_1 and k_2.

In order to make the BEM-based procedures clearer without loss of generality, we here suppose that the temperature boundary conditions are prescribed on external surfaces Γ_1 and Γ_2.

First, the exterior boundary of subdomain Ω_1, as shown in Fig. 2, is analyzed. One has the following discretized form of the BIE given in (1)–(6):

$$[G^1]\begin{Bmatrix}\{\phi^1\}\\ \{\phi_I^1\}\end{Bmatrix}=\{U^1\},\quad [G_I^1]\begin{Bmatrix}\{\phi^1\}\\ \{\phi_I^1\}\end{Bmatrix}=\{U_I^1\} \tag{9a}$$

$$[H^1]\begin{Bmatrix}\{\phi^1\}\\ \{\phi_I^1\}\end{Bmatrix}=\{Q^1\},\quad [H_I^1]\begin{Bmatrix}\{\phi^1\}\\ \{\phi_I^1\}\end{Bmatrix}=\{Q_I^1\} \tag{9b}$$

where U_I^1 and Q_I^1 are the interface temperature and normal derivative of temperature of the subdomain Ω_1 on the interface Γ_I, ϕ^1 the density function on Γ_1, ϕ_I^1 the density function of the subdomain Ω_1 on the interface Γ_I, U^1 and Q^1 the temperature and normal derivative of temperature of the subdomain Ω_1 on the remaining surfaces.

Similarly, for the subdomain Ω_2, we have

$$[G^2]\begin{Bmatrix}\{\phi^2\}\\ \{\phi_I^2\}\end{Bmatrix}=\{U^2\},\quad [G_I^2]\begin{Bmatrix}\{\phi^2\}\\ \{\phi_I^2\}\end{Bmatrix}=\{U_I^2\} \tag{10a}$$

$$[H^2]\begin{Bmatrix}\{\phi^2\}\\ \{\phi_I^2\}\end{Bmatrix}=\{Q^2\},\quad [H_I^2]\begin{Bmatrix}\{\phi^2\}\\ \{\phi_I^2\}\end{Bmatrix}=\{Q_I^2\} \tag{10b}$$

where U_I^2 and Q_I^2 are the interface temperature and normal derivative of temperature of the subdomain Ω_2 on the interface Γ_I, U^2 and Q^2 the temperature and normal derivative of temperature of the subdomain

Ω_2 on the remaining surfaces, ϕ^2 the density function on Γ_2, ϕ_{I}^2 the density function of the subdomain Ω_2 on the interface Γ_{I}.

For a well-posed boundary value problem, there is only unknown (either U or Q) at each nodal point on the boundaries. However, along the interface Γ_{I}, both U and Q are unknowns. To solve the problem numerically, there will be the same number of algebraic equations as the unknowns. Therefore, the following continuity conditions at the interface must be considered:

(a) Continuity of temperature on Γ_{I}:

$$U_{\mathrm{I}}^1 = U_{\mathrm{I}}^2 \tag{11}$$

(b) Continuity of normal flux on Γ_{I}:

$$k_1 Q_{\mathrm{I}}^1 = -k_2 Q_{\mathrm{I}}^2 \tag{12}$$

According to the equilibrium and compatibility conditions (11) and (12) at the interface, discretized algebraic equations (9) and (10) can be coupled as

$$\begin{pmatrix} [G^1] & [0] \\ [G_I^1] & -[G_I^2] \\ [H_I^1] & \frac{k_2}{k_1}[H_I^2] \\ [0] & [G^2] \end{pmatrix} \begin{bmatrix} \begin{pmatrix} \{\phi^1\} \\ \{\phi_I^1\} \end{pmatrix} \\ \begin{pmatrix} \{\phi^2\} \\ \{\phi_I^2\} \end{pmatrix} \end{bmatrix} = \begin{bmatrix} \{U^1\} \\ \{0\} \\ \{0\} \\ \{U^2\} \end{bmatrix} \tag{13}$$

More equations will be added to this system in a similar way for multi-coating problems. The system still needs to be reordered according to the prescribed temperature and normal flux boundary conditions. The system of equations (13) can be solved simultaneously for the boundary and interface unknowns. Once the boundary unknowns are solved, Eqs. (7) and (8) can be integrated to obtain the temperature distributions at any point inside each subdomain.

Note that, the traditional Gaussian quadrature is directly used to calculate the density function in the algebraic equation (13) in the conventional boundary element method (CBEM). However, if the coating of a considered cutting tool is thin, some discretized boundaries will be very close to each other. Thus, the distance r between some boundary nodes and integral elements probably approaches zero. This would cause the coefficients of matrices G^1, G_{I}^1, H_{I}^1 in (13) present various orders of near singularities, and the density functions cannot be calculated accurately by using the traditional Gauss quadrature. Therefore, calculation of the physical quantities at interior points also needs special care. On the other hand, almost all the interior points in thin coatings are very close to the integral elements. Thus, there also exist nearly singular integrals in Eqs. (7) and (8).

The above mentioned nearly singular integrals can be expressed as the following generalized integrals:

$$\begin{cases} I_1 = \int_\Gamma \psi(\boldsymbol{x}) \ln r^2 \, d\boldsymbol{\Gamma} \\ I_2 = \int_\Gamma \psi(\boldsymbol{x}) \dfrac{1}{r^{2\alpha}} \, d\boldsymbol{\Gamma} \end{cases} \tag{14}$$

where $\alpha > 0$, $\psi(\boldsymbol{x})$ is a well-behaved function including the Jacobian, the shape functions and ones that arise from taking the derivative of the integral kernels. Under such a circumstance, either a very fine mesh with massive integration points or a special integration technique needs to be adopted. In the last two decades, numerous research works have been published on this subject in the BEM literature. Most of the work has been focused on the numerical approaches, such as subdivisions of the element of integration, adaptive integration schemes, exact integration methods and so on. However, most of these earlier methods are either inefficient or cannot provide accurate results when the thickness of the thin structure is smaller than 10^{-6}. In this work, a very efficient transformation method is proposed to avoid the integration difficulty for thin coatings with the thickness to length ratio in micro- or nano-scales.

3. Nearly singular integrals under curvilinear elements

The quintessence of the BEM is to discretize the boundary into a finite number of segments, not necessarily equal, which are called boundary elements. Two approximations are made over each of these elements. One is about the geometry of the boundary, while the other has to do with the variation of the unknown boundary quantity over the element. The linear element is not an ideal one as it cannot approximate with sufficient accuracy for the geometry of curvilinear boundaries. For this reason, it is recommended to use higher order elements, namely, elements that approximate geometry and boundary quantities by higher order interpolation polynomials—usually of second order. In this paper, the geometry segment is modeled by a continuous parabolic element, which has three knots, two of which are placed at the extreme ends and the third somewhere in-between, usually at the mid-point. Therefore the boundary geometry is approximated by a continuous piecewise parabolic curve. On the other hand, the distribution of the boundary quantity on each of these elements is depicted by a discontinuous quadratic element, three nodes of which are located away from the endpoints.

Assume $\boldsymbol{x}^1 = (x_1^1, x_2^1)$ and $\boldsymbol{x}^2 = (x_1^2, x_2^2)$ are the two extreme points of the segment Γ_j, and $\boldsymbol{x}^3 = (x_1^3, x_2^3)$ is in-between one. Then the element Γ_j can be expressed as follows:

$$x_k(\xi) = N_1(\xi)x_k^1 + N_2(\xi)x_k^2 + N_3(\xi)x_k^3, \quad k = 1,2 \tag{15}$$

where $N_1(\xi) = \xi(\xi-1)/2$, $N_2(\xi) = \xi(\xi+1)/2$, $N_3(\xi) = (1-\xi)(1+\xi)$, $-1 \le \xi \le 1$.

As shown in Fig. 3, the minimum distance d from the field point $\boldsymbol{y} = (y_1, y_2)$ to the boundary element Γ_j is defined as the length of $\overline{\boldsymbol{y}\boldsymbol{x}^p}$, which is perpendicular to the tangential line $\boldsymbol{t}$ and through the projection point $\boldsymbol{x}^p$. Letting $\eta \in (-1,1)$ is the local coordinate of the projection point $\boldsymbol{x}^p$, i.e. $\boldsymbol{x}^p = (x_1(\eta), x_2(\eta))$. Then η is the real root of the following equation:

$$x_k'(\eta)(x_k(\eta) - y_k) = 0 \tag{16}$$

If the field point $\boldsymbol{y}$ sufficiently approaches the boundary, then Eq. (16) has a unique real root. In fact, setting

$$F(\eta) = x_k'(\eta)(x_k(\eta) - y_k)$$

there is

$$F'(\eta) = x_k'(\eta)x_k'(\eta) + x''_k(\eta)(x_k(\eta) - y_k) = J^2(\eta) + x''_k(\eta)(x_k(\eta) - y_k)$$

where $J(\eta)$ is the Jacobian of the transformation from parabolic element to the line interval $[-1,1]$. Therefore, when the field point $\boldsymbol{y}$ is sufficiently close to the element, we explicitly have $F'(\eta) > 0$.

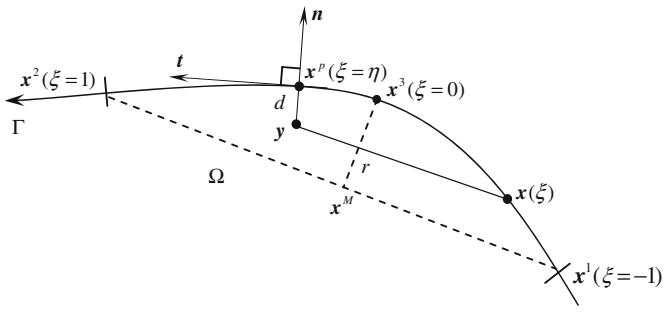

Fig. 3. The minimum distance d from the field point $\boldsymbol{y}$ to the boundary element.

The unique real root of Eq. (16) can be evaluated numerically by using the Newton's method or computed exactly by adopting the algebraic root formulas of 3rd algebraic equations. In this paper, two ways are all tested, and practical applications show that both ways can be used to obtain desired results. Furthermore, the Newton's method is more simple and effective, especially if the initial approximation is properly chosen and if we can do this, only two or three iterations are sufficient to approximate the real root. For the root formula of 3rd algebraic equations, let us consider the following algebraic equation:

$$ax^3+bx^2+cx+d=0$$

if there exists only one real root, the analytical solution can be expressed as follows:

$$x=-\frac{b}{3a}+\frac{2\left(\sqrt{s^2+t^2}\right)^{1/3}}{3\sqrt[3]{2a}}\cos\left(\frac{1}{3}\arccos\frac{s}{\sqrt{s^2+t^2}}\right)$$

where $s=-2b^3+9acb-27a^2d$,

$t=\sqrt{-4(3ac-b^2)^3-(-2b^3+9acb-27a^2d)^2}$.

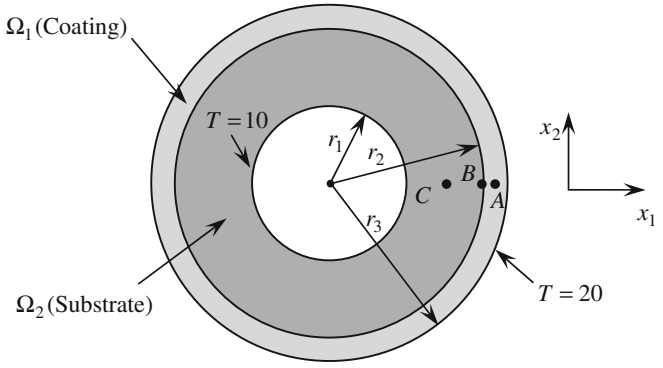

Fig. 4. Cross section of a shaft with a thin coating.

Using the procedures described above, we can obtain the value of the real root η. Thus, we have

$$x_k-y_k=x_k-x_k^p+x_k^p-y_k=\frac{1}{2}(\xi-\eta)\left[(x_k^1-2x_k^3+x_k^2)(\xi+\eta)+(x_k^2-x_k^1)\right]+x_k(\eta)-y_k \tag{17}$$

By using Eq. (17), the distance square r^2 between the field point $\boldsymbol{y}$ and the source point $\boldsymbol{x}(\xi)$ can be written as

$$r^2(\xi)=(x_k-y_k)(x_k-y_k)=(\xi-\eta)^2g(\xi)+d^2 \tag{18}$$

where $d^2=(x_k(\eta)-y_k)(x_k(\eta)-y_k)$

$$g(\xi)=\frac{1}{4}(x_k^1-2x_k^3+x_k^2)(x_k^1-2x_k^3+x_k^2)(\xi+\eta)^2+\frac{1}{2}(x_k^1-2x_k^3+x_k^2)(x_k^2-x_k^1)(\xi+\eta)+h^2+(x_k^1-2x_k^3+x_k^2)(x_k(\eta)-y_k),\text{where}$$

$$h=\frac{1}{2}\sqrt{(x_k^2-x_k^1)(x_k^2-x_k^1)}$$

Apparently, there is $g(\xi)\geq 0$.

By some simple deductions, the nearly singular integrals in Eq. (14) can be reduced to the following two types:

$$\begin{cases} I_1=\int_{-1}^{1} f(\xi)\ln\left[(\xi-\eta)^2g(\xi)+d^2\right]d\xi \\ I_2=\int_{-1}^{1}\dfrac{f(\xi)}{\left[(\xi-\eta)^2g(\xi)+d^2\right]^{\alpha}}d\xi \end{cases} \tag{19}$$

where $f(\cdot)$ is a regular function that consists of shape function, Jacobian, and ones which arise from taking the derivative of the integral kernels. It is obvious that the above integrals would present various orders of near singularity if d is very small. The key to achieving high accuracy is to find an algorithm to calculate these integrals accurately for a small value of d.

Table 1
Results of temperatures at the point A in the domain Ω_1.

$(r_3-r_2)/r_1$	Exact	CBEM	Relative error (%)	Present	Relative error (%)
1.0E−01	0.1846705E+02	0.1846820E+02	−0.6231714E−02	0.1846830E+02	−0.6758478E−02
1.0E−02	0.1977389E+02	0.1954567E+02	0.1154139E+01	0.1977404E+02	−0.7531768E−03
1.0E−03	0.1997628E+02	0.1795833E+02	0.1010176E+02	0.1997629E+02	−0.1885485E−04
1.0E−04	0.1999762E+02	0.1558630E+02	0.2205923E+02	0.1999761E+02	0.5266084E−04
1.0E−05	0.1999976E+02	0.1506173E+02	0.2469045E+02	0.1999975E+02	0.5978710E−04
1.0E−06	0.1999998E+02	0.1500866E+02	0.2495660E+02	0.1999996E+02	0.6050036E−04
1.0E−07	0.2000000E+02	0.1500528E+02	0.2497359E+02	0.1999999E+02	0.6057122E−04
1.0E−08	0.2000000E+02	0.1499499E+02	0.2502505E+02	0.1999999E+02	0.6057561E−04
1.0E−09	0.2000000E+02	0.1497120E+02	0.2514399E+02	0.1999999E+02	0.6056653E−04
1.0E−10	0.2000000E+02	0.1494523E+02	0.2527384E+02	0.1999999E+02	0.6053826E−04

Table 2
Results of fluxes $\partial T/\partial x_1$ at the point A in the domain Ω_1.

$(r_3-r_2)/r_1$	Exact	CBEM	Relative error (%)	Present	Relative error (%)
1.0E−01	0.3132081E+01	0.3131908E+01	0.5541639E−02	0.3131919E+01	0.5200833E−02
1.0E−02	0.4532361E+01	0.2996638E+01	0.3388350E+02	0.4531794E+01	0.1250955E−01
1.0E−03	0.4744335E+01	0.1056759E+01	0.7772588E+02	0.4743731E+01	0.1273312E−01
1.0E−04	0.4766628E+01	0.1163437E+01	0.1244080E+03	0.4766126E+01	0.1051473E−01
1.0E−05	0.4768868E+01	0.5210141E+00	0.1109253E+03	0.4768008E+01	0.1804674E−01
1.0E−06	0.4769093E+01	0.6550840E−01	0.1013736E+03	0.4767268E+01	0.3826259E−01
1.0E−07	0.4769115E+01	0.6883414E−02	0.1001443E+03	0.4768719E+01	0.8308074E−02
1.0E−08	0.4769117E+01	0.2444019E−02	0.9994875E+02	0.4773356E+01	0.8888261E−01
1.0E−09	0.4769118E+01	0.5601441E−02	0.9988255E+02	0.4778376E+01	0.1941299E+00
1.0E−10	0.4769122E+01	0.1781746E−02	0.1000374E+03	0.4780034E+01	0.2288118E+00

4. The transformation for nearly singular integrals

The nearly singular integrals in Eq. (19) can be divided into two parts at point η as follows:

$$I_1 = \left\{ \int_{-1}^{\eta} + \int_{\eta}^{1} \right\} f(\xi) \ln\left[(\xi-\eta)^2 g(\xi) + d^2\right] d\xi \tag{20}$$

$$I_2 = \left\{ \int_{-1}^{\eta} + \int_{\eta}^{1} \right\} \frac{f(\xi)}{\left[(\xi-\eta)^2 g(\xi) + d^2\right]^{\alpha}} d\xi \tag{21}$$

By some simple deductions, the integrals in Eqs. (20) and (21) can be reduced to the following forms:

$$I_1 = \int_0^{a_1} \tilde{f}_1(\xi_1) \ln\left[\xi_1^2 \tilde{g}_1(\xi_1) + d^2\right] d\xi_1 + \int_0^{a_2} \tilde{f}_2(\xi_2) \ln\left[\xi_2^2 \tilde{g}_2(\xi_2) + d^2\right] d\xi_2 \tag{22}$$

$$I_2 = \int_0^{a_1} \frac{\tilde{f}_1(\xi_1)}{\left[\xi_1^2 \tilde{g}_1(\xi_1) + d^2\right]^{\alpha}} d\xi_1 + \int_0^{a_2} \frac{\tilde{f}_2(\xi_2)}{\left[\xi_2^2 \tilde{g}_2(\xi_2) + d^2\right]^{\alpha}} d\xi_2 \tag{23}$$

where $\xi_1 = \eta - \xi$, $\xi_2 = \xi - \eta$, $a_1 = 1 + \eta$, $a_2 = 1 - \eta$.

Introducing the following variable transformation

$$\xi_i = d(e^{k_i(1+t)} - 1), \quad i = 1,2 \tag{24}$$

where $k_i = \frac{1}{2}\ln(1 + (a_i/d))$, we can map $\xi_i(0, a_i)$ to $t(-1,1)$.

Substituting (24) into (22) and (23), then Eqs. (22) and (23) can be rewritten as

$$I_1 = dk_1 \int_{-1}^{1} f_1(t) \ln\left[(e^{k_1(1+t)} - 1)^2 g_1(t) + 1\right] e^{k_1(1+t)} dt + dk_1 \int_{-1}^{1} f_1(t) \ln d^2 e^{k_1(1+t)} dt$$

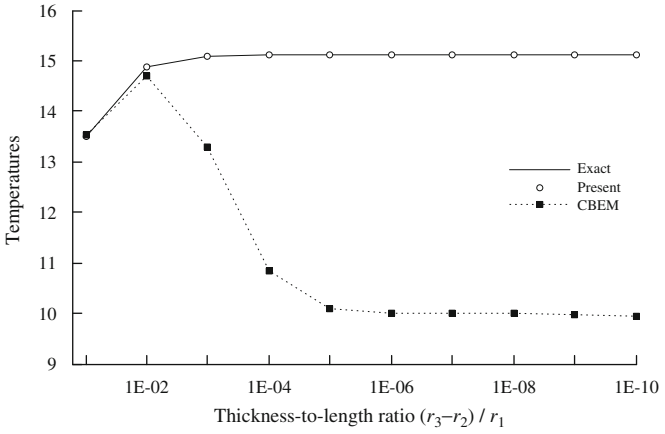

Fig. 5. Results of temperatures at the point C in the domain Ω_2.

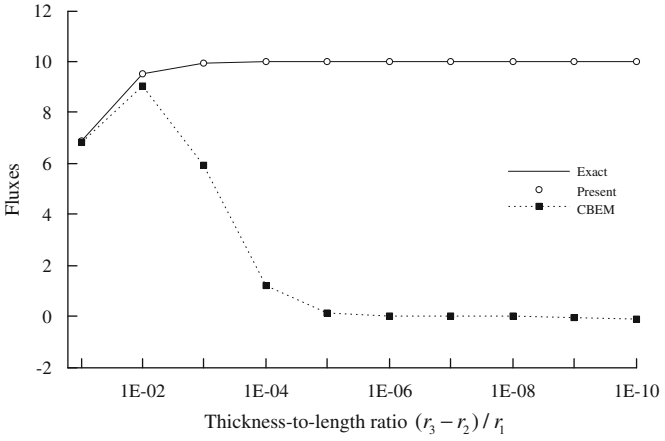

Fig. 6. Results of fluxes $\partial T/\partial x_1$ at the point C in the domain Ω_2.

Table 3
Results of temperatures at the point B in the interface of domains Ω_1 and Ω_2.

$(r_3-r_2)/r_1$	Exact	CBEM	Relative error (%)	Present	Relative error (%)
1.0E−01	0.1686594E+02	0.1686795E+02	−0.1190594E−01	0.1686795E+02	−0.1192834E−01
1.0E−02	0.1954676E+02	0.1907841E+02	0.2396030E+01	0.1954705E+02	−0.1468819E−02
1.0E−03	0.1995256E+02	0.1580660E+02	0.2077908E+02	0.1995256E+02	−0.3807003E−04
1.0E−04	0.1999523E+02	0.1106799E+02	0.4464686E+02	0.1999521E+02	0.1045727E−03
1.0E−05	0.1999952E+02	0.1010611E+02	0.4946826E+02	0.1999950E+02	0.1188223E−03
1.0E−06	0.1999995E+02	0.1001529E+02	0.4992341E+02	0.1999993E+02	0.1202490E−03
1.0E−07	0.2000000E+02	0.1001003E+02	0.4994986E+02	0.1999997E+02	0.1203917E−03
1.0E−08	0.2000000E+02	0.9990413E+01	0.5004793E+02	0.1999998E+02	0.1204057E−03
1.0E−09	0.2000000E+02	0.9944868E+01	0.5027566E+02	0.1999998E+02	0.1204069E−03
1.0E−10	0.2000000E+02	0.9895194E+01	0.5052403E+02	0.1999998E+02	0.1204068E−03

Table 4
Results of normal fluxes $\partial T/\partial n$ at the point B in the interface of domains Ω_1 and Ω_2.

$(r_3-r_2)/r_1$	Exact	CBEM	Relative error (%)	Present	Relative error (%)
1.0E−01	0.6548898E+01	0.6546801E+01	0.3201660E−01	0.6546808E+01	0.3190413E−01
1.0E−02	0.9105925E+01	0.8409471E+01	0.7648362E+01	0.9100165E+01	0.6325216E−01
1.0E−03	0.9492983E+01	0.3865038E+01	0.5928531E+02	0.9486709E+01	0.6608956E−01
1.0E−04	0.9533689E+01	0.5203181E+00	0.1054577E+03	0.9527363E+01	0.6634726E−01
1.0E−05	0.9537780E+01	0.1528142E+00	0.1016022E+03	0.9531450E+01	0.6637273E−01
1.0E−06	0.9538190E+01	0.1512037E−01	0.1001585E+03	0.9531859E+01	0.6637528E−01
1.0E−07	0.9538231E+01	0.1768267E−02	0.9998146E+02	0.9531900E+01	0.6637536E−01
1.0E−08	0.9538235E+01	0.2832121E−02	0.1000297E+03	0.9531904E+01	0.6637651E−01
1.0E−09	0.9538236E+01	0.1668181E−01	0.1001749E+03	0.9531904E+01	0.6638850E−01
1.0E−10	0.9538244E+01	0.3103467E−01	0.1003254E+03	0.9531904E+01	0.6646671E−01

$$+dk_2\int_{-1}^{1} f_2(t)\ln\left[(e^{k_2(1+t)}-1)^2 g_2(t)+1\right]e^{k_2(1+t)}dt$$
$$+dk_2\int_{-1}^{1} f_2(t)\ln d^2 e^{k_2(1+t)}dt \quad (25)$$

$$I_2 = k_1 d^{1-2\alpha}\int_{-1}^{1}\frac{f_1(t)e^{k_1(1+t)}}{\left[(e^{k_1(1+t)}-1)^2 g_1(t)+1\right]^{\alpha}}dt + k_2 d^{1-2\alpha}$$
$$\int_{-1}^{1}\frac{f_2(t)e^{k_2(1+t)}}{\left[(e^{k_2(1+t)}-1)^2 g_2(t)+1\right]^{\alpha}}dt \quad (26)$$

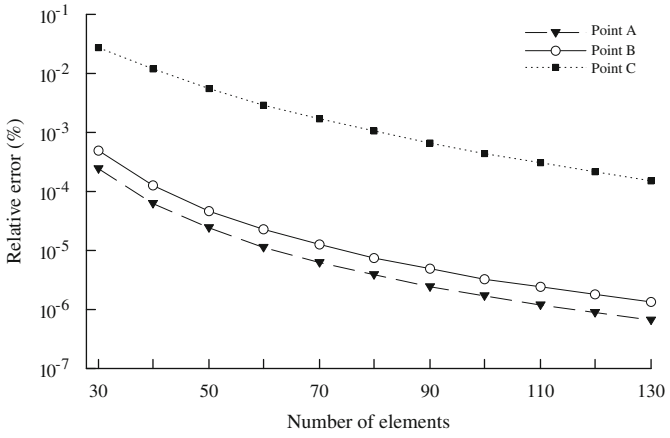

Fig. 7. Convergence curves of the computed temperature at points *A*, *B*, and *C*.

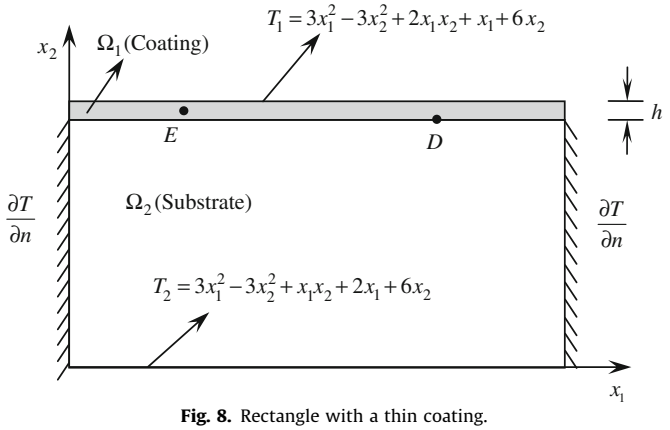

Fig. 8. Rectangle with a thin coating.

where $f_i(t)=f[\eta+(-1)^i d(e^{k_i(1+t)}-1)]$, $g_i(t)=g[\eta+(-1)^i d(e^{k_i(1+t)}-1)]$, $i=1,2$.

We know that the denominator always $(e^{k(1+t)}-1)^2 g(t)+1 \geq 1$ if $g(x)>0$ is a regular function as assumed above. Thus, the integrand is fully regular even if the value of d is very small.

By following the procedures described above, the near singularity of the boundary integrals has been fully regularized even if the thickness of the coatings is in the orders of $10^{-6}-10^{-9}$. The final integral formulations over parabolic elements are obtained as shown in Eqs. (25) and (26), which can now be computed straightforward by using the standard Gaussian quadrature.

5. Numerical examples

To verify the method developed above, two simplified coating test cases are studied in which BEM solutions are compared with the exact solutions.

5.1. Test problem 1: a thin coating on a shaft

In the first test case, which is depicted in Fig. 4, a circular shaft with a thin coating is studied. The mediums of domains Ω_1 and Ω_2 are assumed to, respectively, have heat conductivities of $k_1=2$ and $k_2=1$ W/mK. The inner and outer radii of the domain Ω_2 are $r_1=10$ and $r_2=11$, respectively. The domain Ω_1 is considered to be the coating with an outer radius r_3. The given boundary conditions are temperatures $T_1=20$ on the coating's outer surface and $T_2=10$ on the substrate's inner surface. From the theory of heat transfer, the analytical temperature solutions are given by

$$T_1(x) = T_1 + \frac{C-T_1}{\ln(r_2/r_3)}\ln\frac{r}{r_3} \quad \text{for the domain } \Omega_1$$

$$T_2(x) = T_2 + \frac{C-T_2}{\ln(r_2/r_1)}\ln\frac{r}{r_1} \quad \text{for the domain } \Omega_2$$

where

$$C = \frac{MT_1K_1/K_2 - T_2}{MK_1/K_2 - 1}, \quad M = \frac{\ln(r_2/r_1)}{\ln(r_2/r_3)}$$

here r denotes the radius of the considered points.

There are 10 quadratic boundary elements divided along the inner surface, and 15 uniform quadratic boundary elements on the outer and contact interface surfaces, respectively. Therefore the total number of the elements is 40. Quadratic discontinuous interpolation is adopted to approximate the boundary functions.

In this example, $(r_3-r_2)/r_1$ is defined as the thickness-to-length ratio. As r_1 and r_2 are fixed, the ratio reduces as r_3 decreases. To the authors' knowledge, there does not exist any work in the literature for determining the temperature

Table 5
Results of normal fluxes $\partial T/\partial n$ at the point D in the interface of domains Ω_1 and Ω_2.

h	Exact	CBEM	Relative error (%)	Present	Relative error (%)
1.0E−01	0.3000000E+01	0.2998325E+01	0.5583312E−01	0.2999972E+01	0.9283084E−03
1.0E−02	0.3000000E+01	0.3032585E+01	−0.1086175E+01	0.2999787E+01	0.7085004E−02
1.0E−03	0.3000000E+01	0.3527544E+00	0.8824152E+02	0.3000048E+01	−0.1610846E−02
1.0E−04	0.3000000E+01	−0.1733515E+01	0.1577838E+03	0.3000024E+01	−0.8152285E−03
1.0E−05	0.3000000E+01	−0.2577272E+01	0.1859091E+03	0.2998634E+01	0.4554992E-01
1.0E−06	0.3000000E+01	−0.2663291E+01	0.1887764E+03	0.2998325E+01	0.5583312E−01
1.0E−07	0.3000000E+01	−0.2671899E+01	0.1890633E+03	0.2999276E+01	0.2412128E−01
1.0E−08	0.3000000E+01	−0.2672760E+01	0.1890920E+03	0.2998910E+01	0.3631889E−01
1.0E−09	0.3000000E+01	−0.2672846E+01	0.1890949E+03	0.3001953E+01	0.6510119E−01
1.0E−10	0.3000000E+01	−0.2672855E+01	0.1890952E+03	0.2975448E+01	0.8184141E+00

distribution in the coating layers of the coated cutting tool using the BEM-based simulation. In this numerical test, the physical quantities in the coatings and substrates are considered. For different thickness-to-length ratios, the temperatures and fluxes $\partial T/\partial x_1$ at the interior point $A((r_2+r_3)/2,0)$ in the domain Ω_1 are listed in Tables 1 and 2, respectively. The temperatures and normal fluxes $\partial T/\partial n$ at the point $B(r_2,0)$ in the interface of the domains Ω_1 and Ω_2 are listed in Tables 3 and 4, respectively. The temperatures and fluxes $\partial T/\partial x_1$ at the interior point $C((r_1+r_2)/2,0)$ in the domain Ω_2 are shown in Figs. 5 and 6, respectively.

For quantities in thin coating layers, Tables 1 and 2 show that the CBEM can only be available to calculate the acceptable temperatures and fluxes results for the thickness-to-length ratio down to 1.0E−2. In contrast with the CBEM, the present method can be used to obtain the accurate temperatures and fluxes results at the point A even when the thickness-to-length ratio decreases to 1.0E−10, which is sufficient for modeling most thin coatings in the micro- or nano-scales.

For quantities in the interface of domain Ω_1 and Ω_2, Tables 3 and 4 demonstrate that the temperatures and fluxes results obtained by using the CBEM are unacceptable for the relative errors (%) already greater than 20% when the thickness-to-length ratio smaller than 1.0E−3. Nevertheless, the present method yields highly accurate results with the largest relative error (%) less than 0.07% even when the thickness-to-length ratio as small as 1.0E−10.

The same results of quantities in the domain Ω_2 can be found in Figs. 5 and 6. The convergence curves of computed temperatures at points A, B, and C are shown in Fig. 7, from which we can observe that the convergence rate is fast even when the thickness-to-length ratio reaches 1.0E−9. In Fig. 7, only the errors of the present method are given, since the errors of the CBEM are relatively too large.

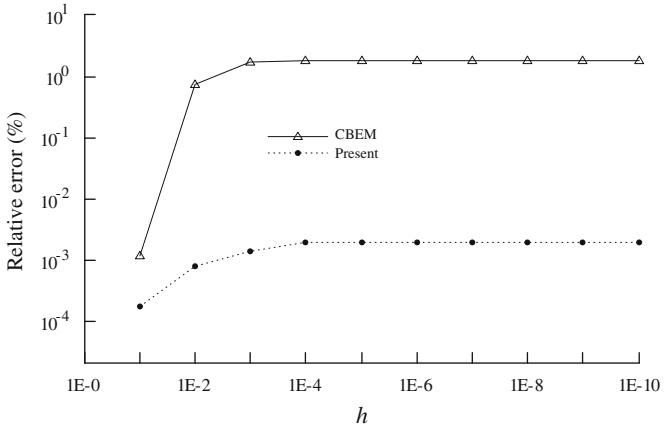

Fig. 9. Relative errors (%) of the calculated temperatures at the point E.

5.2. Test problem 2: a thin coating on a rectangle

In the second test case, we construct a configuration that is closer to a real machining process. As shown in Fig. 8, a 2×1 m^2 rectangle with a thin coating of thickness h is considered. The boundary conditions specified in Fig. 8 are complicated enough to ensure two-dimensional heat transfer. In 2001, Du et al. [4] considered a similar coating test case, in which the exact solution is $T=x_2/(1+h)$. By contrast, the test case presented in this paper is more general, and thus the numerical results are expected to be more accurate if the example in Ref. [4] is revisited.

In this example, the domain Ω_1 is considered to be the coating layer and Ω_2 is its substrate counterpart. The domain Ω_1 and Ω_2 are assumed to have heat conductivities of $k_1=1$ and $k_2=2$ W/mK, respectively.

For the subdomain Ω_1, there are 6 uniform linear elements on the each horizontal long side, 1 linear element are divided on each vertical short side. For the subdomain Ω_2, there are 6 linear elements on the each boundary. Therefore, the total number of elements is 38. When the thickness h ranges from 1.0E−1 to 1.0E−10, the normal fluxes $\partial T/\partial n$ at the point $D(1.5,1)$ in the interface of domain Ω_1 and Ω_2 are listed in Table 5. It is obvious that the results calculated by using the CBEM deteriorate quickly as the thickness is less than 1.0E−2. In contrast, the results

Table 6
Results of fluxes $\partial T/\partial x_1$ at the point E in the domain Ω_1.

h	Exact	CBEM	Relative error (%)	Present	Relative error (%)
1.0E−01	0.6100000E+01	0.6099934E+01	0.1083194E−02	0.6099934E+01	0.1083194E−02
1.0E−02	0.6010000E+01	0.5872755E+01	0.2283614E+01	0.6007734E+01	0.3770990E−01
1.0E−03	0.6001000E+01	−0.1115987E+01	0.1185967E+03	0.5997616E+01	0.5639012E−01
1.0E−04	0.6000100E+01	−0.1780758E+01	0.1296788E+03	0.5996694E+01	0.5676661E−01
1.0E−05	0.6000010E+01	−0.1774198E+01	0.1295699E+03	0.5996604E+01	0.5676015E−01
1.0E−06	0.6000001E+01	−0.1772776E+01	0.1295463E+03	0.5996595E+01	0.5675930E−01
1.0E−07	0.6000000E+01	−0.1772626E+01	0.1295438E+03	0.5996595E+01	0.5675921E−01
1.0E−08	0.6000000E+01	−0.1772611E+01	0.1295435E+03	0.5996594E+01	0.5675930E−01
1.0E−09	0.6000000E+01	−0.1772610E+01	0.1295435E+03	0.5996594E+01	0.5675847E−01
1.0E−10	0.6000000E+01	−0.1772610E+01	0.1295435E+03	0.5996598E+01	0.5669722E−01

Table 7
Fluxes $\partial T/\partial x_1$ at the point of the coating layer on the line $x_1=0.5$.

x_2	Exact	CBEM	Relative error (%)	Present	Relative error (%)
1.0000000001	0.600E+01	−0.1772610E+01	0.1295435E+03	0.5996594E+01	0.5677398E−01
1.0000000002	0.600E+01	−0.1772610E+01	0.1295435E+03	0.5996595E+01	0.5675678E−01
1.0000000003	0.600E+01	−0.1772610E+01	0.1295435E+03	0.5996594E+01	0.5676058E−01
1.0000000004	0.600E+01	−0.1772610E+01	0.1295435E+03	0.5996595E+01	0.5675604E−01
1.0000000006	0.600E+01	−0.1772610E+01	0.1295435E+03	0.5996595E+01	0.5675625E−01
1.0000000007	0.600E+01	−0.1772610E+01	0.1295435E+03	0.5996594E+01	0.5676028E−01
1.0000000008	0.600E+01	−0.1772610E+01	0.1295435E+03	0.5996595E+01	0.5675642E−01
1.0000000009	0.600E+01	−0.1772610E+01	0.1295435E+03	0.5996594E+01	0.5677060E−01

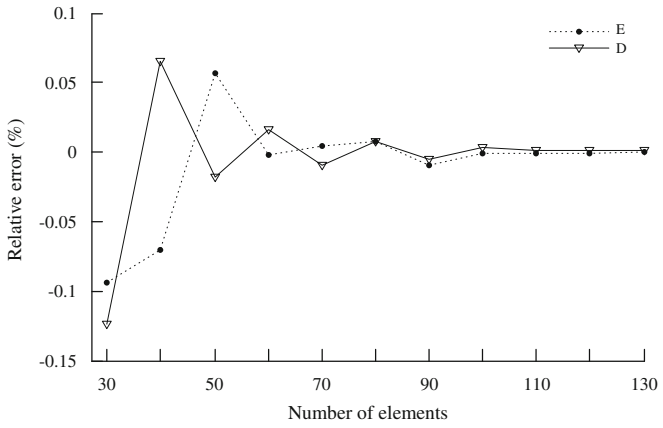

Fig. 10. Convergence curves of the computed fluxes at points *D* and *E*.

calculated by using the proposed method are very consistent with the exact solutions even though the thickness is small as 1.0E−10. The temperatures and fluxes $\partial T/\partial x_1$ at the point $E(0.5,\ 1+h/2)$ are shown in Fig. 9 and Table 6, respectively. For $h=1.0\text{E}-9$, the fluxes $\partial T/\partial x_1$ at the point of the coating layer on the line $x_1=0.5$ are listed in Table 7. These results calculated by using the present BEM are all in good agreement with the exact solutions. However, the CBEM cannot yield acceptable results as the thickness decreases.

For $h=1.0\text{E}-9$, convergence curves of the fluxes at points *D* and *E* calculated by using the presented method are shown in Fig. 10. We can observe that the convergence rate is fast even when the thickness-to-length ratio is small as 1.0E−9.

6. Conclusions

In this work, the multi-domain boundary element techniques were developed for determining the temperature distribution in materials containing thin coating films. In contrast with the previous works in the literature, the proposed BEM-based algorithm has the following specific features:

1. The nearly singular integrals in the BIE can be evaluated accurately even if the thickness to length ratio of the coated film is smaller than the order of 1.0E−9, which is sufficient for modeling most thin coatings in the micro- or nano-scales.
2. Both temperatures and temperature gradients, not only in the substrate but also in the coated layer, are well studied in this paper. The difficult task of determining the temperature distributions in thin coated structures can be dealt with effectively and efficiently.
3. High-order elements to discretize the geometry of the considered domain are adopted when nearly singular integrals need to be calculated. To the authors' best knowledge, no similar work in the literature can be found to efficiently calculate the nearly singular integrals occurring on high-order geometry elements. Owing to the employment of the high-order elements, only a small number of elements need to be divided along the boundary. High accuracy can be achieved without increasing other computational efforts.

This BEM-based approach can be extended easily to model multi-layered coatings, for analyzing contact stresses, interfacial cracks, thermal effects, and nonlinear deformations. All of these topics can be dealt with effectively and efficiently by using the BEM. Some work along this line for thin structures is already underway.

Acknowledgements

The research is supported by the National Natural Science Foundation of China (no. 10571110) and the Natural Science Foundation of Shandong Province of China (no. 2003ZX12).

References

[1] Grzesik W, Bartoszuk M, Nieslony P. Finite difference analysis of the thermal behaviour of coated tools in orthogonal cutting of steels. Int J Mach Tools Manuf 2004;44(14):1451–62.
[2] Chandra A, Chan CL. Thermal aspects of machining: a BEM approach. Int J Solids Struct 1994;31:1657–93.
[3] Stephenson DA, Jen TC, Lavine AS. Cutting tool temperatures in contour turning: transient analysis and experimental verification. J Manuf Sci Eng 1997;119:494–501.
[4] Du F, Lovell MR, Wu TW. Boundary element method analysis of temperature fields in coated cutting tools. Int J Solids Struct 2001;38:4557–70.
[5] Brebbia CA. The boundary element method for engineers. London, New York: Pentech Press, Halstead Press; 1978.
[6] Tanaka M, Sladek V, Sladek J. Regularization techniques applied to BEM. Appl Mech Rev 1994;47(10):457–99.
[7] Sladek V, Sladek J. Singular integrals in boundary element methods. Computational Mechanics Publications; 1998.
[8] Guiggiani M, Krishnasamy G, Rudolphi TJ, Rizzo FJ. A general algorithm for the numerical solution of hypersingular BEM. J Appl Mech 1992;59:604–27.
[9] Liu YJ. On the simple solution and non-singular nature of the BIE/BEM—a review and some new results. Eng Anal Bound Elem 2000;24:286–92.
[10] Chen JT, Chen YW. Dual boundary element analysis using complex variables for potential problems with or without a degenerate boundary. Eng Anal Bound Elem 2000;24(9):671–84.
[11] Chen JT, Lee JW, Cheng YC. On the spurious eigensolutions for the real-part boundary element method. Eng Anal Bound Elem 2009;33(3):342–55.
[12] Zhang JM, Yao ZH. The regular hybrid boundary node method for three-dimensional linear elasticity. Eng Anal Bound Elem 2004;28(5):525–34.
[13] Zhang YM, Wen WD. A kind of new nonsingular boundary integral equations for elastic plane problems. Acta Mech 2004;36(3):311–21. [in Chinese].
[14] Zhang YM, Lü HX. Novel regularized boundary integral equations for potential plane problems. Appl Math Mech 2006;9:1017–22. [in Chinese].
[15] Sun HC, Zhang LZ, Xu Q, Zhang YM. Nonsingular boundary element method. Dalian: Dalian University of Technology Press; 1999. [in Chinese].
[16] Cruse TA. An improved boundary integral equation method for three dimensional elastic stress analysis. Comput Struct 1974;4:741–54.
[17] Lachat JC, Watson JO. Effective numerical treatment of boundary integral equation: a formulation for elastostatics. Int J Numer Methods Eng 1976;21:211–28.
[18] Chen HB, Lu P, Huang MG, Williams FW. An effective method for finding values on and near boundaries in the elastic BEM. Comput Struct 1998;69(4):421–31.
[19] Granados JJ, Gallego G. Regularization of nearly hypersingular integrals in the boundary element method. Eng Anal Bound Elem 2001;25:165–84.
[20] Jun L, Beer G, Meek JL. Efficient evaluation of integrals of order using Gauss quadrature. Eng Anal 1985;2:118–123.
[21] Gao XW, Yang K, Wang J. An adaptive element subdivision technique for evaluation of various 2D singular boundary integrals. Eng Anal Bound Elem 2008;32:692–6.
[22] Earlin L. Exact Gaussian quadrature methods for near-singular integrals in the boundary element method. Eng Anal Bound Elem 1992;9:233–45.
[23] Liu YJ. Analysis of shell-like structures by the boundary element method based on 3-D elasticity: formulation and verification. Int J Numer Methods Eng 1998;41:541–58.
[24] Yoon SS, Heister SD. Analytic solution for fluxes at interior points for 2D Laplace equation. Eng Anal Bound Elem 2000;24:155–60.
[25] Niu ZR, Cheng CZ, Zhou HL, Hu ZJ. Analytic formulations for calculating nearly singular integrals in two-dimensional BEM. Eng Anal Bound Elem 2007;31:949–64.
[26] Zhou HL, Niu ZR, Cheng CZ, Guan ZW. Analytical integral algorithm applied to boundary layer effect and thin body effect in BEM for anisotropic potential problems. Comput Struct 2008;86:1656–71.
[27] Telles JCF. A self-adaptive coordinate transformation for efficient numerical evaluation of general boundary element integral. Int J Numer Methods Eng 1987;24:959–73.
[28] Johnston PR. Application of sigmoidal transformations to weakly singular and near singular boundary element integrals. Int J Numer Methods Eng 1999;45:1333–48.
[29] Sladek V, Sladek J, Tanaka M. Optimal transformations of the integration variables in computation of singular integrals in BEM. Int J Numer Methods Eng 2000;47:1263–83.
[30] Earlin L. A mapping method for numerical evaluation of two-dimensional integrals with singularity. Comput Mech 1993;12:19–26.

[31] Huang Q, Cruse TA. Some notes on singular integral techniques in boundary element analysis. Int J Numer Methods Eng 1993;36:2643–59.
[32] Ma H, Kamiya N. Distance transformation for the numerical evaluation of near singular boundary integrals with various kernels in boundary element method. Eng Anal Bound Elem 2002;26:329–39.
[33] Zhang YM, Gu Y. An effective method in BEM for potential problems of thin bodies. J Mar Sci Technol 2010;18(1):137–44.
[34] Zhang YM, Sun CL. A general algorithm for the numerical evaluation of nearly singular boundary integrals in the equivalent non-singular BIES with indirect unknowns. J Chin Inst Eng 2008;31:437–47.
[35] Zhang YM, Gu Y, Chen JT. Boundary layer effect in BEM with high order geometry elements using transformation. CMES 2009;45(3):227–47.
[36] Zhang YM, Gu Y, Chen JT. Analysis of 2D thin walled structures in BEM with high-order geometry elements using exact integration. CMES 2009;50(1):1–20.